Effects of Transition-Metal Mixing on Na Ordering and Kinetics in Layered P2 Oxides

Chen Zheng, Balachandran Radhakrishnan, Iek-Heng Chu, Zhenbin Wang, and Shyue Ping Ong

Phys. Rev. Applied **7**, 064003 — Published 6 June 2017

DOI: 10.1103/PhysRevApplied.7.064003

Effect of Transition Metal Mixing on Na Ordering and Kinetics in Layered P2 Oxides

Chen Zheng, Balachandran Radhakrishnan, Iek-Heng Chu, Zhenbin Wang, and Shyue Ping Ong*

Department of NanoEngineering, University of California San Diego, 9500 Gilman Dr, Mail Code 0448, La Jolla, CA 92093-0448, United States

Abstract

Layered P2 oxides are promising cathode materials for rechargeable sodium-ion batteries. In this work, we systematically investigate the effect of transition metal (TM) mixing on Na ordering and kinetics in the $Na_xCo_{1-y}Mn_yO_2$ model system using density functional theory (DFT) calculations. The DFT predicted 0K stability diagrams indicate that Co-Mn mixing reduces the energetic differences between Na orderings, which may account for the reduction of the number of phase transformations observed during cycling of mixed TM P2 layered oxides compared to single TM. Using ab initio molecular dynamics simulations and nudged elastic band calculations, we show that the TM composition at the Na(1) (face-sharing) site has a strong influence on the Na site energies, which in turns impacts the kinetics of Na diffusion towards the end of charge. By employing a site percolation model, we establish theoretical upper and lower bounds for TM concentration based on their effect on Na(1) site energies, providing a framework to rationally tune mixed TM compositions for optimal Na diffusion.

* ongsp@eng.ucsd.edu

I. INTRODUCTION

Rechargeable sodium-ion batteries (SIBs) have recently emerged as promising candidates for large-scale energy storage applications.[1–3] Sodium (2.3% of the Earth's crust) is three orders of magnitude more abundant than lithium (0.0017%).[4, 5] More importantly, sodium-ion battery chemistry enables new cell designs that can potentially yield significant advantages over lithium-ion chemistry. For instance, the possibility of using Al foil as anode current collector instead of the more expensive Cu makes it probable that Na-ion batteries can be produced at less than half the cost of Li-ion.[6] Also, a great variety of sodium superionic conductors are known,[7–10] paving the way for the potential development of all-solid-state Na-ion batteries that may be safer with higher energy density than traditional architectures based on organic liquid electrolytes.

One of the key challenges in SIBs is the development of cathodes with sufficiently high voltage and capacity. The most promising candidates are the layered sodium transition metal (TM) oxides Na_xMO_2, which have been extensively investigated as cathodes in SIBs due to their excellent electrochemical performance.[11–23] Here, M can either be a single TM, *e.g.*, Co, Ni, Mn, Fe, V, Cr, or a mixture of these TMs, sometimes with other elements such as Li. Unlike the layered $LiMO_2$, which only exists in the O3 polymorph, Na_xMO_2 compounds exist in both the P2 and O3 stackings. In this stacking classification first proposed by Delmas *et al.* [24], P and O denote the environment occupied by the alkali atom (prismatic and octahedral, respectively) between the MO_6 octahedral stacking sheets, while the numerals 2 and 3 refer to the number of MO_2 layers per repeating unit. P2 Na_xMO_2 generally outperform their O3 analogs in terms of the reversible capacity and cyclability.[3]

The P2 Na_xMO_2 crystal structure is shown in Figure 1. Na in P2 Na_xMO_2 can occupy two types of sites: the Na(1) site shares faces with two MO_6 octahedra, and the Na(2) site which only shares edges with MO_6 octahedra. Adjacent Na(1) and Na(2) sites cannot be occupied simultaneously due to strong Coulombic repulsion.

For the single TM P2 Na_xCoO_2 and P2 Na_xMnO_2,[25, 26] potential drops related to the formation of biphasic states during the charge/discharge processes indicate the existence of dominant Na orderings across the entire Na insertion/deinsertion range. These orderings, especially for P2 Na_xCoO_2, have been extensively investigated using both experimental and computational approaches.[27–32] The presence of ordered intermediate phases plays a

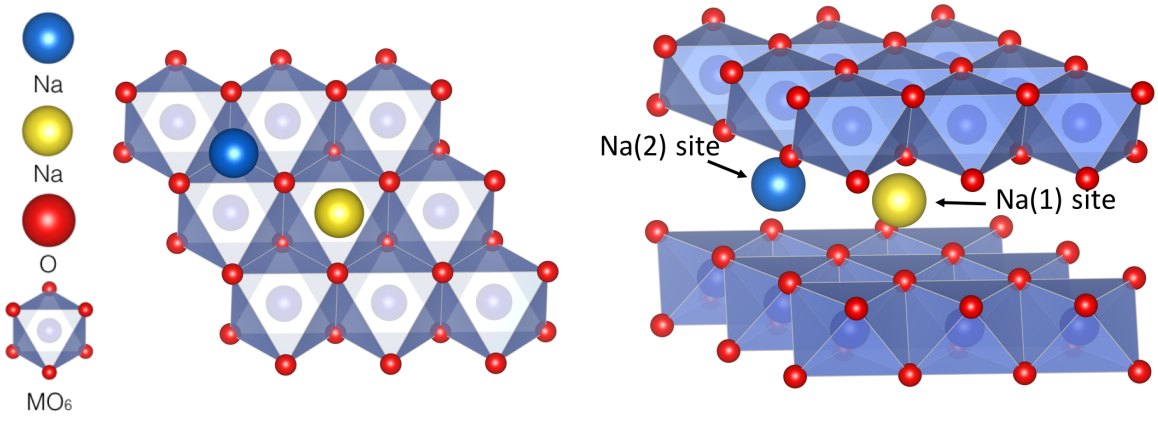

(a)View along [001] direction (b)Perspective view

FIG. 1: Crystal structure of P2 Na_xMO_2 with ABBA-type Layer Stacking. Na occupies two distinct prismatic sites: the Na(1) site (yellow) shares faces with two MO_6 octahedra and the Na(2) site (blue) shares only edges.

critical role in the electrochemical performance of P2 cathodes, as highly favored orderings may introduce kinetic limitations that may in turn limit the achievable capacity.

Various mixed TM P2 $Na_xM_yM'_{1-y}O_2$ and $Na_xM_yM'_zM''_{1-y-z}O_2$ have been investigated [2, 13, 14, 33–36] with the aim of eliminating phase transformations during the charge/discharge process and extending the stability of the P2 phase over a wider Na intercalation region. Studies of binary or ternary TM P2 compounds suggest that Mn mixing can suppress the occurrence of long range sodium orderings.[3, 14, 36] Recent studies on series of P2 Na_xMO_2 (M=Co, Mn) also suggest that a small amount of Co substitution with Mn in P2 Na_xCoO_2 reduces the formation of stable Na orderings at certain Na concentrations, and results in the solid-solution-like behavior over a wide range of Na compositions.[37, 38]

Previous computational studies have shown that the Na-ion diffusion in O3 layered Na_xMO_2 can be as facile as the Li analog,[1] even though the difference in ionic radius between Na^+ (1.02 Å) and Li^+ (0.76 Å) is substantial.[39–41] Mo *et al.* [41] has also demonstrated using ab initio molecular dynamics (AIMD) simulations that P2 Na_xCoO_2 exhibit excellent Na conductivity over a wide range of Na concentrations. More recently, Guo and co-workers[42, 43] showed that there is a strong correlation between the crystal structure and the Na diffusion in P-type $Na_{0.62}Ti_{0.37}Cr_{0.63}O_2$. In addition, the investigation of Na-ion conductivity in different compounds at interphase layer of SIBs has been carried out using

a combined experimental and theoretical approach.[44]

In this work, we present a density functional theory (DFT) study on the effect of transition metal mixing on Na ordering and kinetics in layered P2 oxides using $Na_xCo_{1-y}Mn_yO_2$ as a model system. The choice of the P2 $Na_xCo_{1-y}Mn_yO_2$ system is motivated by the fact that this system has been well-studied in experiments,[14, 37, 38] providing a wealth of data for comparison and validation. We will demonstrate that Co-Mn mixing reduces the energetic differences between Na orderings, and present a theoretical framework to tune mixed TM compositions for optimal Na kinetics.

II. METHODS

A. Structure enumeration

All symmetrically distinct Na orderings in P2 $Na_xCo_{1-y}Mn_yO_2$ for $y = 0, 1/3, 2/3, 1$ were enumerated using the algorithm of Hart and Forcade [45]. For the single TM systems ($y = 0, 1$), enumerations were carried out at both 1/8 and 1/6 Na concentration intervals, *i.e.*, $x = 0, 1/8, 1/6, 1/4, 1/3, 3/8, 1/2, 5/8, 2/3, 3/4, 5/6, 7/8, 1$. For the mixed TM systems, enumerations were carried out only at 1/6 Na concentration intervals, *i.e.*, $x = 0, 1/6, 1/3, 1/2, 2/3, 5/6, 1$, due to the lower symmetry of these systems. For each y, we first determined the lowest energy Na, Co and Mn orderings at $x = 2/3$ within a $\sqrt{3}a \times \sqrt{3}b \times c$ supercell (Figure 2(b)) to mimic initial synthesis Na concentrations of layered P2 cathodes. The supercell we used is comparable to those used in previous first-principles investigations of layered Na TM oxides.[29, 46] The lowest energy Co-Mn ordering at each y is then retained at all other Na concentrations x. We note that it has been well-established experimentally that Co and Mn generally forms a solid solution in this system,[38, 47] and we will discuss the implications of fixing the Co-Mn ordering in the Results section.

To keep the number of orderings manageable, we adopted the following constraints in performing the enumeration of Na orderings at different Na concentrations:

- Three supercell sizes that comprise up to twelve formula units (f.u.), as shown in Figure 2, were used.
- Each P2 cell comprises two Na layers. For the mixed TM systems, the Na concentrations in both layers were constrained to be equal to limit the total number of orderings.

- Although Na can occupy both Na(1) and Na(2) sites, simultaneous occupation of adjacent Na(1) and Na(2) sites is not allowed. Due to the large coulombic repulsion between Na^+, these structures are likely to be of too high energy to be of any interest.

In total, structural optimization and total energy calculations of more than 5,000 distinct structures at various Na concentrations and TM mixing ratios were performed using an automated workflow implemented with the Fireworks scientific workflow software.[48] The lowest energy structures of P2 $Na_xCo_{1-y}Mn_yO_2$ were then adopted in subsequent calculations.

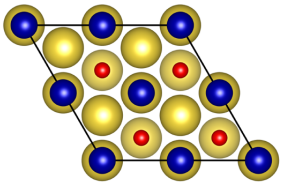

(a)$2a \times 2b \times c$, 8 formula units

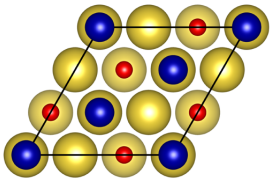

(b)$\sqrt{3}a \times \sqrt{3}b \times c$, 6 formula units

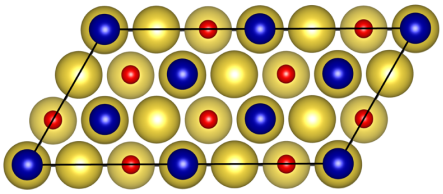

(c)$2\sqrt{3}a \times \sqrt{3}b \times c$, 12 formula units

FIG. 2: Supercells of P2 $Na_xCo_{1-y}Mn_yO_2$ used to enumerate Na and Co/Mn orderings, viewed along the [001] direction. Top view on AB plane.

B. Energy calculations

All DFT energy calculations were performed using the Vienna *Ab initio* simulation package (VASP) within the projector augmented-wave approach.[49, 50] Spin-polarized calculations were performed using a k-point density of at least 1000/(number of atoms in the unit cell) and an energy cutoff of 520 eV. The exchange-correlation functional used was the

Perdew-Burke-Ernzerhof (PBE)[51] generalized-gradient approximation and the Hubbard U extension to it (PBE+U).[52] The spherically averaged scheme of the on-site coulomb interactions was adopted,[53, 54] and effective U values used for Mn and Co were 3.9 eV and 3.32 eV respectively, similar to the values used in the Materials Project.[55] These effective U values are average values that have been well-tested to reproduce the energies of redox energies involving $Mn^{3+/4+}$ and $Co^{3+/4+}$ in accordance to the approach proposed by Wang et al.[53] Co^{3+} and Co^{4+} were initialized in low spin, Mn^{3+} and Mn^{4+} were initialized in high spin, which were found to yield the lowest energy in P2 $Na_xCo_{1-y}Mn_yO_2$. All calculations were initialized in a ferromagnetic configuration,[56] and the total magnetic moment of the unit cell is constrained to the expected value determined from the Na concentration and the consequent oxidation states of Co and Mn.

0K stability diagram. The pseudo-binary 0K stability diagram for each TM-mixing ratio y was constructed by plotting the formation energy of each ordering σ_i at Na concentration x with respect to the fully sodiated and desodiated end members, given by the following equation:

$$\Delta E_f^{\sigma_i} = E(\sigma_i) - xE(NaCo_{1-y}Mn_yO_2) - (1-x)E(Co_{1-y}Mn_yO_2), \tag{1}$$

where $E(\sigma_i)$, $E(NaCo_{1-y}Mn_yO_2)$, and $E(Co_{1-y}Mn_yO_2)$ are the total DFT energies per f.u. of the ordering: σ_i, $NaCo_{1-y}Mn_yO_2$ and $Co_{1-y}Mn_yO_2$, respectively. The stable phases were then identified using the convex hull construction.[57] Because no entropic effects (e.g., vibrational, configurational, etc.) were taken into account, these diagrams are by definition 0K stability diagrams, and not finite-temperature phase diagrams.

Intercalation potential. The average intercalation potential V of cathode between two stable Na ordered phases at Na concentrations x_1 and x_2 was calculated using the following expression:[58]

$$V = -\frac{E(Na_{x_2}Co_{1-y}Mn_yO_2) - E(Na_{x_1}Co_{1-y}Mn_yO_2) - (x_2-x_1)E(Na)}{(x_2-x_1)e}, \tag{2}$$

where E is the DFT total energy and e is the electronic charge.

C. Ab initio molecular dynamics simulations

Ab initio molecular dynamics (AIMD) simulations were carried out in the constant volume (NVT) ensemble at 1000 K with a Nose-Hoover thermostat.[59, 60] The aim of these calculations is not to obtain converged statistics for an estimate of the diffusivity, but rather to elucidate the Na site occupancies and diffusion mechanisms in P2 $Na_{1/2}Co_{1-y}Mn_yO_2$, $0 \leq y \leq 1$ at non-dilute Na concentrations. As such, these calculations were performed at a single, relatively high temperature (no melting was observed in our simulations), and simulations were carried out for a relatively short time of 80 ps. To reduce computational costs, all AIMD simulations were non-spin-polarized, and a smaller plane wave energy cutoff of 300 eV and Γ-centered $1 \times 1 \times 1$ k-point grid were employed. Supercells of $4 \times 4 \times 1$ (32 formula units) and $3\sqrt{3} \times 2\sqrt{3} \times 1$ (36 formula units) were used for the single and mixed TM systems respectively. The time step of simulations was 2 fs. The initial models for the simulations were obtained by removing half of the Na atoms in each Na layer from fully sodiated structures to model compounds at Na concentration $x = 1/2$.

D. Climbing-image nudged elastic band calculations

Na migration barriers were calculated using the climbing image nudged elastic band method (CI-NEB).[61, 62] The PBE GGA functional was adopted in the NEB calculations to exclude the impact of electron transfer on the diffusion barrier calculation.[1] Supercells of $4 \times 4 \times 1$ (32 formula units) and $2\sqrt{3} \times 2\sqrt{3} \times 1$ (24 formula units) were used for mixed and single TM systems respectively. A Γ-centered $2 \times 2 \times 2$ k-points grid was used, and each interpolated image was relaxed until the forces on each atom were less than 0.05 eV $Å^{-1}$.

At dilute Na concentration, to isolate the role of transition metal on Na diffusion, different Na(1) site configurations were created in the lattice of CoO_2 with Ni, Mn and Fe as dopants. Na migration barriers from a Na(2) site to its nearest Na(2) site via different Na(1) sites were evaluated. We also adopted the $Co_{2/3}Mn_{1/3}O_2$ framework to study the influence of Ni dopant on Na migration energy in the P2 ternary TM oxides.

All analyses were performed using the Python Materials Genomics (pymatgen) package.[63].

III. RESULTS

A. 0K stability diagram and Na ordering

1. $NaCoO_2$

The stability diagram, Na ordering and diffusion in P2 Na_xCoO_2 have been extensively investigated through DFT calculations[28–32, 41] and electrochemical characterization.[26, 64] Figure 3 shows the computed 0K stability diagrams of Na_xCoO_2 using the PBE and PBE+U functionals. These 0K stability diagrams are in good agreement with previous studies. Stable orderings of Na_xCoO_2 are found at $x = 1/8, 1/4, 1/3, 1/2, 2/3, 3/4$ with the PBE approximation, as shown in Figure 3(a). Although our study did not identify any stable orderings at $x = 5/6$ and $x = 7/8$, the formation energy of the lowest energy orderings at these concentrations are within 10 meV f.u.$^{-1}$ of the convex hull. The two stable Na orderings previously reported by Berthelot *et al.* [26] at these concentrations require larger supercells than those used in our high-throughput study. Nevertheless, these high Na concentration compositions are of less practical interest given that the layered P2 materials are typically synthesized at $x \leq 0.75$. For the PBE+U functional, stable Na orderings are found at the same Na concentrations as the PBE functional, with the exception of $x = 1/8$. Also, the lowest energy orderings at $x = 5/6$ and $x = 7/8$ are significantly higher in energy above the convex hull (56 meV f.u.$^{-1}$ and 45 meV f.u.$^{-1}$, respectively), consistent with previous works.[26, 28]

Despite the better qualitative agreement of the stable Na orderings calculated without the Hubbard U parameter, especially at lower Na concentrations, we find that PBE+U reproduces absolute voltages much better than PBE (Figure 3(c)). This is due to the better self-interaction error cancellation for the redox reaction with the application of the Hubbard U.[65] The agreement between our DFT predicted voltage profiles and experimental studies is on par with the previous first-principles investigation of the P2 systems.[28]

2. $NaMnO_2$

Figures S1(a) and S1(b) show the PBE and PBE+U 0K stability diagrams of Na_xMnO_2. The stable Na orderings with both functionals are given in Figures S2 and S3 in the Supple-

mentary Information.[81] Although the Na concentrations at which stable orderings occur are the same in PBE and PBE+U, we find considerable differences in the predicted stable Na orderings at $x = 1/2$. The PBE+U ground state for $Na_{1/2}MnO_2$ has only Na(2) sites occupied, while the PBE ground state shows characteristic "row" motifs formed by alternating Na(1) and Na(2) lines, similar to $Na_{1/2}CoO_2$. The difference in orderings is likely due to a greater energy penalty associated with the face-sharing Na(1) sites due to the Jahn-Teller distortion of Mn^{3+}, which is better captured with the application of the Hubbard U.[66, 67]

To our knowledge, the experimental stability diagram of P2 Na_xMnO_2 has not been previously reported because O3 Na_xMnO_2 is significantly more stable than the P2 structure at low temperatures.[25, 68, 69] Similar to $NaCoO_2$, we find that the PBE+U voltages are in much better agreement with experimental voltages compared to PBE (see Figure S1(c)).

3. $Na_xCo_{1-y}Mn_yO_2$, $y = \frac{1}{3}, \frac{2}{3}$

For $Na_xCo_{1-y}Mn_yO_2$, we will discuss mainly the PBE+U results. With the presence of a non-negligible amount of Mn, these systems are likely to exhibit strong $3d$ localization, for which the application of the Hubbard U is appropriate. The PBE (no U) results are given in Figures S4 and S5 in the Supplementary Information[81] for interested readers. Figure S6 shows the lowest energy $Na_xCo_{1-y}Mn_yO_2$ structures at $x = 2/3$ and $y = 1/3, 2/3$. We find that the lowest energy structures in both instances exhibit a hexagonal ordering pattern similar to that observed in other mixed TM layered P2 systems. It is well-established in the experimental literature[14, 38, 47] that the mixed Co-Mn system tends to exhibit solid solution behavior, i.e., no superstructure ordering is observed for Co and Mn. Indeed, we find that the Co-Mn ordering has a small effect on relative energies, regardless of the specific Na ordering (see Table S1 and S2 in the SI).

From Figures 4(a) and 4(b), we make the observation that the mixed TM $Na_xCo_{1-y}Mn_yO_2$ are characterized by the presence of many meta-stable orderings whose energies are within 30 meV f.u.$^{-1}$ of the convex hull. This is unlike the single TM Na_xMO_2 (Figures 3(b) and S1(b)), which exhibit distinct stable Na orderings that are substantially lower in energy compared to other orderings, *i.e.*, there is a large energy gap between the ground state ordering and the next lowest energy ordering.

Figure 4(c) and Figure 4(d) compare the PBE+U voltage profiles for $Na_xCo_{2/3}Mn_{1/3}O_2$

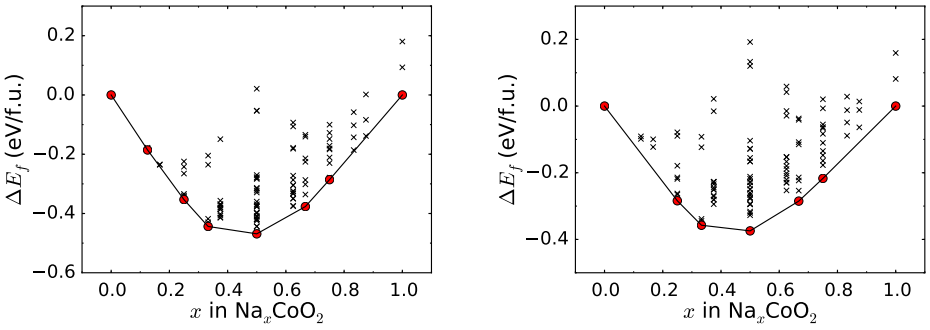

(a)PBE 0K stability diagram (b)PBE+U 0K stability diagram

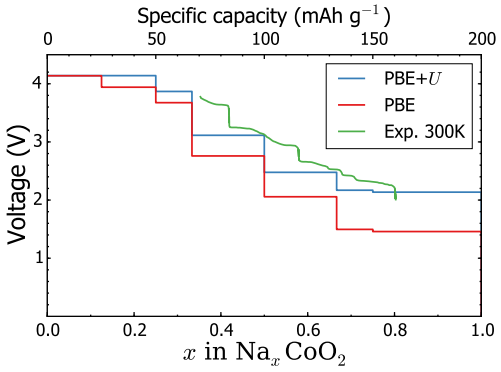

(c)Voltage profile

FIG. 3: (a) PBE and (b) PBE+U 0K stability diagrams of Na_xCoO_2. Black line: convex hull; red dots: stable orderings; black cross: unstable orderings. (c) Comparison of PBE and PBE+U voltage profiles with the experimental data from Ref. 26.

and $Na_xCo_{1/3}Mn_{2/3}O_2$ with the electrochemically measured voltage profiles of Wang *et al.* [14] Again, we find that the calculated voltages are in relatively good agreement with the experimental ones. For $Na_xCo_{2/3}Mn_{1/3}O_2$, the small potential drop at $x = 1/2$ in the PBE+U voltage profile indicates the formation of a stable ordered phase during deintercalation/intercalation process, in agreement with previous experiments.[14, 38] It should be noted that for $Na_xCo_{1/3}Mn_{2/3}O_2$, we have shifted the experimental voltage curve by -0.2 Na concentration to properly align the computed and experimental voltage profiles. This shift accounts for the artificial over-sodiation (which results in Na stoichiometry > 1 in experiments) observed in the electrochemical measurements.[14]

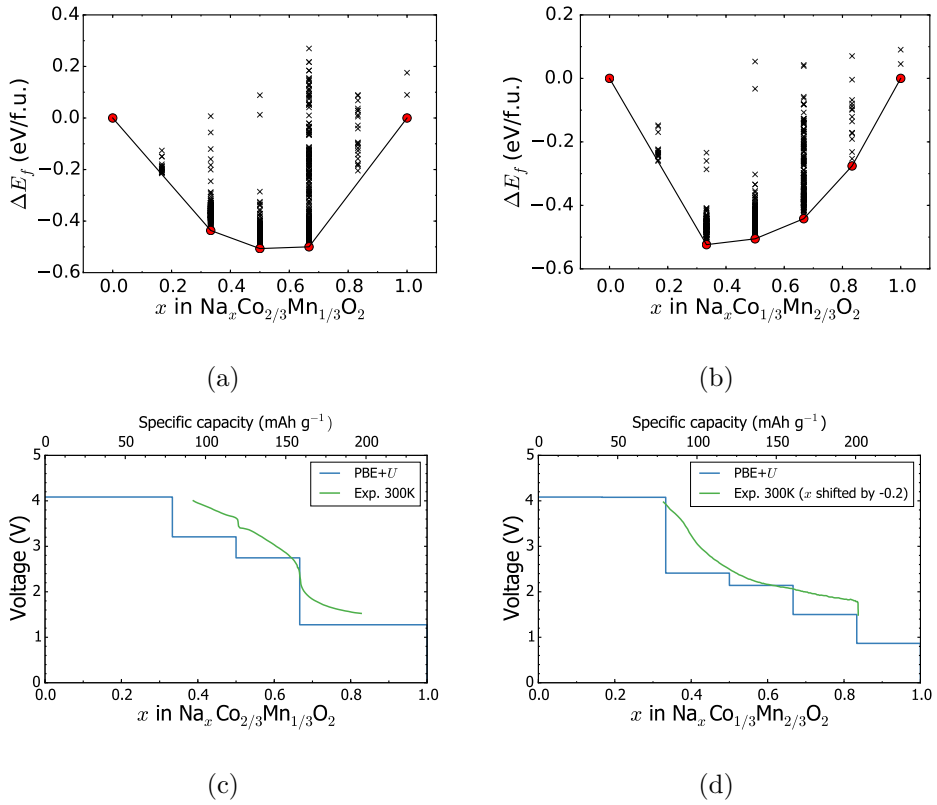

FIG. 4: PBE+U 0K stability diagrams of (a) $Na_xCo_{2/3}Mn_{1/3}O_2$ 0K stability diagram and (b) $Na_xCo_{1/3}Mn_{2/3}O_2$ 0K stability diagram. The solid black line shows the convex hull with red dots representing stable orderings on the hull. The black cross dots show unstable orderings. Panels (c) and (d) show the comparison between PBE+U and experimental voltage profiles of $Na_xCo_{1-y}Mn_yO_2$ for $y = 1/3$ and $2/3$. Experimental voltage profiles for $Na_xCo_{2/3}Mn_{1/3}O_2$ and $Na_xCo_{1/3}Mn_{2/3}O_2$ (x shifted by -0.2) are from refs 38 and 14, respectively.

B. Na diffusion kinetics

To identify the effect of TM mixing on Na kinetics, we performed AIMD simulations on $Na_xCo_{1-y}Mn_yO_2$ at single Na concentration of $x = 1/2$ and Mn concentrations of $y = 0, 1/6, 1/3, 1/2, 2/3$ and 1 in our study. The choice of $x = 1/2$ is motivated by the fact that strong Na orderings are typically observed at that Na concentration in the single TM, and even in mixed TM systems, which may have a significant effect on Na kinetics.

We classify the Na sites of $Na_{1/2}Co_{1-y}Mn_yO_2$ into four types according to our Co-Mn

frameworks.

1. Na(2), which shares only edges with MO_6 octahedra.

2. $Na(1)_{Mn-Mn}$, which shares faces with two MnO_6 octahedra.

3. $Na(1)_{Co-Co}$, which shares faces with two CoO_6 octahedra.

4. $Na(1)_{Co-Mn}$, which shares faces with one CoO_6 octahedra and one MnO_6 octahedra.

Figure 5 shows the isosurfaces of the Na probability density distribution extracted from the AIMD simulations of the ground state TM orderings. The probability density distribution was calculated by averaging the Na occupation on a uniform grid over the trajectories during AIMD simulations of 25 ps. As can be observed from Figure S8, thermal equilibration was achieved for all systems after 10 ps of simulation time, and the relevant statistics were obtained after this equilibration period. In the ground state orderings of $y = 1/3$ and $2/3$, all Na sites either share edges with MO_6 octahedra, or share faces with only one type of TM, i.e., there are no $Na(1)_{Co-Mn}$ sites. We will relax this constraint shortly. We may observe that the Na trajectories in the single TM (Figures 5(a) and 5(b)) exhibit the typical honeycomb network observed in previous studies.[41] At $y = 1/3$ (Figure 5(d)), we observe that there is a clear preference for Na diffusion to occur via the Na(2) and $Na(1)_{Co-Co}$ sites, which form a percolating diffusion network, while the $Na(1)_{Mn-Mn}$ is clearly less preferred. At higher concentration of Mn ($y = 2/3$, Figure 5(g)), the Na trajectories once again follow the honeycomb topology given that a percolating diffusion network cannot be formed from Na(2) and $Na(1)_{Co-Co}$ sites.

To obtain a more quantitative assessment of site preferences, the Na site occupancy fractions (SOFs) were estimated from the AIMD trajectories for the four kinds of sites in $Na_{1/2}Co_{1-y}Mn_yO_2$. Each Na is assigned to the closest site within the Na honeycomb network. The average Na SOFs are then given by:

$$\mathrm{SOF(t)} = \frac{1}{\mathrm{tN_d}} \int_0^{\mathrm{t}} \mathrm{N_i(t')dt'}, \tag{3}$$

wherein $N_i(t')$ is the total number of Na^+ ions in sites of type i at time t' and N_d is the total number of Na^+ ions in the system.

Figure 6 summarizes the average Na SOFs. Here, we have presented the results for additional AIMD simulation of $y = 1/3$ structure where the Co-Mn ordering has been randomized in such a way that it contains all four types of Na sites (denoted as $y = 1/3^*$). We notice that the randomized TM ordering and the ground state one are close in energy for $Na_{1/2}Co_{2/3}Mn_{1/3}O_2$ with identical Na ordering (< 10 meV atom^{-1}). We may make the following observations:

1. At all Mn concentrations, the Na(2) site is clearly the most preferred site, with an average SOF of ~ 0.6.

2. At $y < 1/2$, we find that $Na(1)_{Co-Co}$ is the next most preferred site, followed by $Na(1)_{Co-Mn}$. $Na(1)_{Mn-Mn}$ is the least preferred. The higher SOF of $Na(1)_{Mn-Mn}$ compared to $Na(1)_{Co-Mn}$ at $y = 1/3$ is an artifact as the ground state $y = 1/3$ ordering does not contain $Na(1)_{Co-Mn}$ sites. When the Co-Mn ordering is randomized ($y = 1/3^*$), the SOF of $Na(1)_{Co-Mn}$ is clearly higher than $Na(1)_{Mn-Mn}$.

3. At $y = 1/2$, the SOF of the $Na(1)_{Co-Co}$ decreases substantially given than there are more $Na(1)_{Co-Mn}$ sites. Nevertheless, both $Na(1)_{Co-Mn}$ and $Na(1)_{Co-Co}$ exhibit significantly higher SOFs than $Na(1)_{Mn-Mn}$.

4. Finally, at $y = 2/3$, the much higher concentration of Mn results in an almost equal $Na(1)_{Co-Co}$ and $Na(1)_{Mn-Mn}$ SOF.

IV. DISCUSSION

A. Na ordering in P2 $Na_xCo_{1-y}Mn_yO_2$

We provide an overview of the P2 $Na_xCo_{1-y}Mn_yO_2$ 0K stability diagram as a function of x and y in Figure 7, with the stable orderings indicated by blue circles. The background color indicates the formation energy relative to the fully sodiated and desodiated single TM end points, calculated as:

$$\Delta E_f(\mathrm{Na}_x\mathrm{Co}_{1-y}\mathrm{Mn}_y\mathrm{O}_2) = E(\mathrm{Na}_x\mathrm{Co}_{1-y}\mathrm{Mn}_y\mathrm{O}_2) - x[(1-y)E(\mathrm{NaCoO}_2) + yE(\mathrm{NaMnO}_2)] - (1-x)[(1-y)E(\mathrm{CoO}_2) + yE(\mathrm{MnO}_2)], \quad (4)$$

where $E(X)$ refers to the energy of the phase X. Values between data points are linearly interpolated.

In general, we find that both PBE and PBE+U give stable orderings at similar Na concentrations for each y, especially in the Na concentration range of interest $1/3 \leq x \leq 2/3$. Though there are minor differences in the actual stable ordered structures, the qualitative features of the 0K stability diagrams are generally consistent between PBE and PBE+U. The notable exception is the $\mathrm{Na}_x\mathrm{CoO}_2$ system, for which it has been well-established that the application of the Hubbard U leads to 0K stability diagrams that are in disagreement with experiments at lower x.[28]

From Figure 7, we observe that the formation of mixed Co-Mn phases is very unfavorable (positive formation energies relative to the single TM end members) at close to full sodiation ($x \sim 1$) and desodiation ($x \sim 0$) at 0K. Formation of mixed Co-Mn phases is most favorable at $0.25 \leq x \leq 0.75$. Most mixed TM layered P2 materials are typically synthesized at $x \sim 0.67-0.75$, [13, 14, 22, 23, 36, 38] which is within the the range of x where the predicted formation energies relative to the end members is negative. We also note that the mixed Co-Mn phases are known to be disordered at finite temperatures,[14] and configurational entropic effects are not taken into account in the 0K stability diagram.

Previously, Wang *et al.* [14] have carried out an extensive experimental study of P2 $\mathrm{Na}_x\mathrm{Co}_{1-y}\mathrm{Mn}_y\mathrm{O}_2$. Their findings were that as Co is substituted by Mn, i.e., increasing y, the accessible capacity increases, and a number of ordered states, particularly that at $x = 2/3$, disappear. The computed 0K stability diagrams also predict a large number of nearly degenerate Na orderings upon TM mixing, particularly at $x = 2/3$, which supports these experimental observations. We also find that Co-Mn ordering has a relatively small effect on total energies, regardless of Na ordering, which again supports experimental observations that Co-Mn disorder in this system.[47]

It should be noted that a key limitation of this work is that it is based on 0K DFT calculations of Na orderings up to relatively small supercell sizes, and the effect of temper-

ature are not considered. Na orderings at other compositions that require larger supercell size are not included in our study. For the Na composition range of general interest (i.e. $0.33 < x < 0.75$), however, our predicted stability diagrams and intercalation voltage profiles are in reasonably good agreement with the experimental literature.[14, 26] A possible extension to incorporate these effects to some degree is to fit a cluster expansion Hamiltonian[70] using the calculated energies and perform Monte Carlo simulations[71] on much larger supercell sizes to obtain finite temperature voltage profiles and diffusivities. However, this effort would require accounting not just for Na/vacancy orderings, but also electron/hole orderings for two transition metals. This significant undertaking is outside the scope of this work and would be the subject of future studies.

B. Na migration barriers

From the AIMD simulations and CI-NEB calculations, we have established that the Na(1) site that shares faces with two MnO_6 octahedra ($Na(1)_{Mn-Mn}$) is higher in energy relative to Na(1) sites that share faces with two CoO_6 ($Na(1)_{Co-Co}$) or one CoO_6 and one MnO_6 ($Na(1)_{Co-Mn}$). We will here generalize these results into a universal theoretical framework for the rational optimization of mixed TM layered P2 oxides.

In the layered P2 oxides, Na diffusion occurs in a 2D honeycomb lattice,[41] which can be decomposed into two intersecting triangular lattices comprising Na(2) and Na(1) prismatic sites. The Na(2) sites are generally lower in energy as they only share edges and not faces with MO_6 octahedra. However, diffusion between Na(2) sites must occur via the Na(1) sites. Hence, we may treat the triangular network of the higher-energy Na(1) sites as the effective diffusion topology for P2 layered oxides (Figure 8). From site percolation theory, a long-range percolating diffusion path exists at the macroscopic limit if probability of site occupancy exceeds the percolation threshold p_c. For the triangular network, this threshold can be shown analytically to be 0.5.[72]

Consider the introduction of a new TM species M′ at some concentration z into a layered P2 oxide. M′ can have either a beneficial or detrimental effect on Na diffusion by lowering or increasing the energy of Na(1) sites that share faces with it. Here, we will assume that the new mixed TM P2 layered oxide is disordered, which can occur because of either an intrinsically low enthalpy of mixing or through the synthesis or processing that usually

takes place at elevated temperatures. There are four limiting cases:

1. **M′ has a substantial beneficial effect such that any Na(1) site that share faces with at least one $M'O_6$ has a sufficiently low barrier for diffusion at 300K.** The probability of any Na(1) site having at least one $M'O_6$ is $2z(1-z)+z^2$. The condition for macroscopic fast diffusion is then $2z(1-z)+z^2 > 0.5$, i.e., $z > 0.293$:

2. **M′ has a moderate beneficial effect such that only Na(1) sites that share faces with two $M'O_6$ have a sufficiently low barrier for diffusion at 300K.** The probability of any Na(1) site having two $M'O_6$ is z^2. The condition for macroscopic fast diffusion is then $z^2 > 0.5$, i.e., $z > 0.707$:

3. **M′ has a substantial detrimental effect such that any Na(1) site that share faces with at least one $M'O_6$ has a high barrier for diffusion at 300K.** The probability of any Na(1) site having at least one $M'O_6$ is $2z(1-z)+z^2$. The condition for macroscopic fast diffusion is then $1-(2z(1-z)+z^2) > 0.5$, i.e., $z < 0.293$:

4. **M′ has a moderate detrimental effect such that only Na(1) sites that share faces with two $M'O_6$ have a high barrier for diffusion at 300K.** The probability of any Na(1) site having two $M'O_6$ is z^2. The condition for macroscopic fast diffusion is then $1-z^2 > 0.5$, i.e., $z < 0.707$:

Using CI-NEB calculations, we have calculated the Na(2)-Na(1)-Na(2) (see Figure 8 for path) migration barriers for various Na(1) site compositions. These calculations were performed for a single Na hopping in otherwise empty lattice of P2 $NaCoO_2$, i.e., at the fully charged limit, with different M′ introduced at the Na(1) site. As can be seen from Table I, Mn is indeed predicted to have a detrimental effect on Na diffusion, consistent with the results of the AIMD simulations and SOFs. We find that Fe and Ni are predicted to have a beneficial effect on Na diffusion, i.e., lowering of the Na(1) site energies relative to the pure $NaCoO_2$ at end of charge. We have performed similar calculations using $NaCo_{2/3}Mn_{1/3}O_2$ (see Table S4), and the same qualitative trends in the effect of M′ observed.

Na(1) site TM	NEB barrier (meV)
Co-Co	76
Co-Mn	90
Mn-Mn	100
Co-Fe	63
Fe-Fe	61
Co-Ni	46
Ni-Ni	65

TABLE I: Na migration barriers of different Na(1) site composition.

C. Overall kinetics

From the preceding analyses, we may surmise that TM mixing can have two effects: (i) suppression of Na-vacancy ordering, leading to a wider range of single-phase behavior; and (ii) modification of the Na(1) site energies, and hence diffusion barriers, especially towards the end of charge. The former effect is well-established in the literature, with many experimental works conclusively demonstrating the suppression of Na-vacancy ordering in the Co-Mn[14, 26], Co-Mn-Fe[36], Co-Mn-Ni[73] and other systems. However, the latter effect has not been explored in detail, and indeed, most TM mixing in the search for compositions that offer greater rate capability have been carried out mostly in an trial-and-error fashion thus far.

This work provides a rational basis for the selection of mixed TM compositions by establishing the effect of different TM on Na(1) site energies, and the necessary minimum and maximum limits for beneficial and detrimental TM dopants, respectively. We have indirect

evidence from the experimental literature supporting these conclusions. Most mixed TM P2 layered materials reported with reasonable rate capability thus far have a concentration of Mn, which high Na(1) site energy, of around 0.67,[12, 13, 33, 74–77] close to the upper limit of 0.707 predicted in order for a percolating network of sites that do not contain two Mn to exist. In particular, two reported compositions with high rate performance are $Na_{2/3}Mn_{1/2}Co_{1/4}Fe_{1/4}O_2$[36] and $Na_{2/3}Co_{2/3}Mn_{2/9}Ni_{1/9}O_2$[73], wherein the Mn concentration is well below 0.707. In the case of $Na_{2/3}Co_{2/3}Mn_{2/9}Ni_{1/9}O_2$, the Mn concentration is below 0.293, indicating that a percolating network of Na(1) without Mn exists in this material. Furthermore, the improved rate performance of both these materials compared to $Na_{2/3}CoO_2$[78], P2 $Na_{0.6}MnO_2$[25] and P2 $Na_{2/3}Co_{1-y}Mn_yO_2$[14] suggests that Ni and Fe do indeed have a beneficial effect as suggested by the CI-NEB results.

It should be noted that the above conclusions were based on CI-NEB calculations on model frameworks in the dilute Na (fully charged) limit, and under the assumption of fully disordered TM mixing. No consideration was given to possible effect of TM mixing composition on inter-layer spacing at various Na concentrations, a factor that is known to have a significant effect on diffusion barriers close to the end of charge.[79, 80] Nevertheless, we believe the results provide a useful rational framework to further explore TM composition tuning in the layered P2 oxides. We hope that future systematic experimental investigations would provide quantitative verification (as opposed to the indirect evidence highlighted above) of the effect of the different TM on diffusion barriers, and the concentration limits suggested by our model.

V. CONCLUSION

To conclude, we have performed a first-principles investigation on the Na diffusion kinetics of mixed TM P2 $Na_xCo_{1-y}Mn_yO_2$. The calculated 0K stability diagrams suggest that Co-Mn mixing tends to decrease the energy difference between different Na orderings, which may suppress the formation of strongly ordered intermediates and promote single-phase behavior over a wider range of Na concentration. Using AIMD simulations and CI-NEB calculations, we show that the TM composition at a particular Na(1) site can have a profound effect on the Na site occupation energy. The presence of Mn is shown to lead to an increase in the Na(1) site energy, leading to higher diffusion barriers. Fe and Ni, on the other hand, are

shown to lower Na(1) site energies and diffusion barriers relative to Co. By employing a site percolation model based on Na site occupancy and CI-NEB results, we also establish theoretical upper and lower bounds on the concentration of various TM species based on their beneficial/detrimental effect on Na diffusion barriers at the end of charge. These results provide a useful rational framework for further optimization of TM mixing composition in the P2 layered oxides.

VI. ACKNOWLEDGEMENT

This work was supported by the U.S. Department of Energy, Office of Science, Basic Energy Sciences under Award DE- SC0012118. The computations were performed on the Extreme Science and Engineering Discovery Environment (XSEDE), which is supported by National Science Foundation grant number ACI-1053575.

[1] S. P. Ong, V. L. Chevrier, G. Hautier, A. Jain, C. Moore, S. Kim, X. Ma, and G. Ceder, Voltage, stability and diffusion barrier differences between sodium-ion and lithium-ion intercalation materials, Energy Environ. Sci. **4**, 3680 (2011).

[2] N. Yabuuchi, R. Hara, K. Kubota, J. Paulsen, S. Kumakura, and S. Komaba, A new electrode material for rechargeable sodium batteries: P2-type $Na_{2/3}[Mg_{0.28}Mn_{0.72}]O_2$ with anomalously high reversible capacity, J. Mater. Chem. A **2**, 16851–16855 (2014).

[3] N. Yabuuchi, M. Kajiyama, J. Iwatate, H. Nishikawa, S. Hitomi, R. Okuyama, R. Usui, Y. Yamada, and S. Komaba, P2-type $Na_x[Fe_{1/2}Mn_{1/2}]O_2$ made from earth-abundant elements for rechargeable Na batteries, Nat. Mater. **11**, 512–7 (2012).

[4] T. Shimono, D. Tanabe, W. Kobayashi, and Y. Moritomo, Structural Response of P2-Type Na_xMnO_2 against Na^+ Intercalation, J. Phys. Soc. Jpn. **82**, 083601 (2013).

[5] N. Yabuuchi, K. Kubota, M. Dahbi, and S. Komaba, Research development on sodium-ion batteries, Chem. Rev. **114**, 11636–11682 (2014).

[6] K. Kubota and S. Komaba, Review-Practical Issues and Future Perspective for Na-Ion Batteries, J. Electrochem. Soc. **162**, A2538–A2550 (2015).

[7] A. Hayashi, K. Noi, N. Tanibata, M. Nagao, and M. Tatsumisago, High sodium ion conductivity of glass-ceramic electrolytes with cubic Na_3PS_4, J. Power Sources **258**, 420-423 (2014).

[8] Z. Zhu, I.-H. Chu, Z. Deng, and S. P. Ong, Role of Na^+ Interstitials and Dopants in Enhancing the Na^+ Conductivity of the Cubic Na_3PS_4 Superionic Conductor, Chem. Mater. **27**, 8318–8325 (2015).

[9] K. Nanjundaswamy, A. Padhi, J. Goodenough, S. Okada, H. Ohtsuka, H. Arai, and J. Yamaki, Synthesis, redox potential evaluation and electrochemical characteristics of NASICON-related-3D framework compounds, Solid State Ionics **92**, 1 – 10 (1996).

[10] I.-H. Chu, S. K. Christopher, N. Han, Z. Zhu, H. Sunny, Z. Deng, Y. S. Meng, and S. P. Ong, Room-Temperature All-solid-state Rechargeable Sodium-ion Batteries with a Cl-doped Na_3PS_4 Superionic Conductor, Sci. Rep. **6**, 33733 (2016).

[11] I. Hasa, S. Passerini, and J. Hassoun, A rechargeable sodium-ion battery using a nanostructured Sb-C anode and P2-type layered $Na_{0.6}Ni_{0.22}Fe_{0.11}Mn_{0.66}O_2$ cathode, RSC Adv. **5**, 48928–48934 (2015).

[12] J. Zhao, J. Xu, D. H. Lee, N. Dimov, Y. S. Meng, and S. Okada, Electrochemical and thermal properties of P2-type $Na_{2/3}Fe_{1/3}Mn_{2/3}O2$ for Na-ion batteries, J. Power Sources **264**, 235 – 239 (2014).

[13] H. Yoshida, N. Yabuuchi, K. Kubota, I. Ikeuchi, A. Garsuch, M. Schulz-Dobrick, and S. Komaba, P2-type $Na_{2/3}Ni_{1/3}Mn_{2/3-x}Ti_xO_2$ as a new positive electrode for higher energy Na-ion batteries, Chem. Commun. **50**, 3677–3680 (2014).

[14] X. Wang, M. Tamaru, M. Okubo, and A. Yamada, Electrode Properties of P2-$Na_{2/3}Mn_yCo_{1-y}O_2$ as Cathode Materials for Sodium-Ion Batteries, J. Phys. Chem. C **117**, 15545–15551 (2013).

[15] N. Yabuuchi, M. Yano, H. Yoshida, S. Kuze, and S. Komaba, Synthesis and Electrode Performance of O3-Type $NaFeO_2$-$NaNi_{1/2}Mn_{1/2}O_2$ Solid Solution for Rechargeable Sodium Batteries, J. Electrochem. Soc. **160**, A3131–A3137 (2013).

[16] J. S. Thorne, R. A. Dunlap, and M. N. Obrovac, Structure and Electrochemistry of $Na_xFe_xMn_{1-x}O_2$ ($1.0 \leq x \leq 0.5$) for Na-Ion Battery Positive Electrodes, J. Electrochem. Soc. **160**, A361–A367 (2013).

[17] X. Lu, Y. Wang, P. Liu, L. Gu, Y.-S. Hu, H. Li, G. P. Demopoulos, and L. Chen, Direct imaging of layered O3- and P2-$Na_xFe_{1/2}Mn_{1/2}O_2$ structures at the atomic scale, Phys. Chem.

Chem. Phys. **16**, 21946–21952 (2014).

[18] K. Park, D. Han, H. Kim, W.-s. Chang, B. Choi, B. Anass, and S. Lee, Characterization of a P2-type chelating-agent-assisted $Na_{2/3}Fe_{1/2}Mn_{1/2}O_2$ cathode material for sodium-ion batteries, RSC Adv. **4**, 22798–22802 (2014).

[19] E. Talaie, V. Duffort, H. L. Smith, B. Fultz, and L. F. Nazar, Structure of the high voltage phase of layered P2-$Na_{2/3-z}[Mn_{1/2}Fe_{1/2}]O_2$ and the positive effect of Ni substitution on its stability, Energy Environ. Sci. **8**, 2512–2523 (2015).

[20] Z.-Y. Li, R. Gao, L. Sun, Z. Hu, and X. Liu, Designing an advanced P2-$Na_{0.67}Mn_{0.65}Ni_{0.2}Co_{0.15}O_2$ layered cathode material for Na-ion batteries, J. Mater. Chem. A **3**, 16272–16278 (2015).

[21] B. Mortemard de Boisse, J.-H. Cheng, D. Carlier, M. Guignard, C.-J. Pan, S. Bordere, D. Filimonov, C. Drathen, E. Suard, B.-J. Hwang, A. Wattiaux, and C. Delmas, O3-$Na_xMn_{1/3}Fe_{2/3}O_2$ as a positive electrode material for Na-ion batteries: structural evolutions and redox mechanisms upon Na^+ (de)intercalation, J. Mater. Chem. A **3**, 10976–10989 (2015).

[22] X. Wu, J. Guo, D. Wang, G. Zhong, M. J. McDonald, and Y. Yang, P2-type $Na_{0.66}Ni_{0.33-x}Zn_xMn_{0.67}O_2$ as new high-voltage cathode materials for sodium-ion batteries, J. Power Sources **281**, 18–26 (2015).

[23] J. Ding, Y. Zhou, Q. Sun, X. Yu, X. Yang, and Z. Fu, Electrochemical properties of P2-phase $Na_{0.74}CoO_2$ compounds as cathode material for rechargeable sodium-ion batteries, Electrochim. Acta **87**, 388 – 393 (2013).

[24] C. Delmas, C. Fouassier, and P. Hagenmuller, Structural classification and properties of the layered oxides, Physica B+C **99**, 81 – 85 (1980).

[25] A. Caballero, L. Hernan, J. Morales, L. Sanchez, J. Santos Pena, and M. A. G. Aranda, Synthesis and characterization of high-temperature hexagonal P2-$Na_{0.6}MnO_2$ and its electrochemical behaviour as cathode in sodium cells, J. Mater. Chem. **12**, 1142–1147 (2002).

[26] R. Berthelot, D. Carlier, and C. Delmas, Electrochemical investigation of the P2-Na_xCoO_2 phase diagram, Nat. Mater. **10**, 74–80 (2011).

[27] Q. Huang, M. L. Foo, J. W. Lynn, H. W. Zandbergen, G. Lawes, Y. Wang, B. H. Toby, A. P. Ramirez, N. P. Ong, and R. J. Cava, Low temperature phase transitions and crystal structure of $Na_{0.5}CoO_2$, J. Phys.: Condens. Matter **16**, 5803 (2004).

[28] Y. Hinuma, Y. S. Meng, and G. Ceder, Temperature-concentration phase diagram of P2-Na_xCoO_2 from first-principles calculations, Phys. Rev. B **77**, 224111 (2008).

[29] Y. S. Meng, A. Van der Ven, M. K. Y. Chan, and G. Ceder, *Ab initio* study of sodium ordering in $Na_{0.75}CoO_2$ and its relation to Co^{3+}/Co^{4+} charge ordering, Phys. Rev. B **72**, 172103 (2005).

[30] P. Zhang, R. B. Capaz, M. L. Cohen, and S. G. Louie, Theory of sodium ordering in P2-Na_xCoO_2, Phys. Rev. B **71**, 153102 (2005).

[31] G. J. Shu and F. C. Chou, Sodium-ion diffusion and ordering in single-crystal P2-Na_xCoO_2, Phys. Rev. B **78**, 052101 (2008).

[32] Y. S. Meng, Y. Hinuma, and G. Ceder, An investigation of the sodium patterning in Na_xCoO_2 ($0.5 \leq x \leq 1$) by density functional theory methods, J. Chem. Phys. **128**, 104708 (2008).

[33] J. S. Thorne, R. A. Dunlap, and M. N. Obrovac, Investigation of P2-$Na_{2/3}Mn_{1/3}Fe_{1/3}Co_{1/3}O_2$ for Na-Ion Battery Positive Electrodes, J. Electrochem. Soc. **161**, A2232–A2236 (2014).

[34] D. Kim, S.-H. Kang, M. Slater, S. Rood, J. T. Vaughey, N. Karan, M. Balasubramanian, and C. S. Johnson, Enabling Sodium Batteries Using Lithium-Substituted Sodium Layered Transition Metal Oxide Cathodes, Adv. Energy Mater. **1**, 333–336 (2011).

[35] J. Xu, D. H. Lee, R. J. Clment, X. Yu, M. Leskes, A. J. Pell, G. Pintacuda, X.-Q. Yang, C. P. Grey, and Y. S. Meng, Identifying the Critical Role of Li Substitution in P2-$Na_x[Li_yNi_zMn_{1-y-z}]O_2$ ($0 < x, y, z < 1$) Intercalation Cathode Materials for High-Energy Na-Ion Batteries, Chem. Mater. **26**, 1260–1269 (2014).

[36] L. Liu, X. Li, S.-H. Bo, Y. Wang, H. Chen, N. Twu, D. Wu, and G. Ceder, High-Performance P2-Type $Na_{2/3}(Mn_{1/2}Fe_{1/4}Co_{1/4})O_2$ Cathode Material with Superior Rate Capability for Na-Ion Batteries, Adv. Energy Mater. **5**, 1500944–n/a (2015).

[37] J.-H. Cheng, C.-J. Pan, J.-F. Lee, J.-M. Chen, M. Guignard, C. Delmas, D. Carlier, and B.-J. Hwang, Simultaneous Reduction of Co^{3+} and Mn^{4+} in P2-$Na_{2/3}Co_{2/3}Mn_{1/3}O_2$ As Evidenced by X-ray Absorption Spectroscopy during Electrochemical Sodium Intercalation, Chem. Mater. **26**, 1219–1225 (2014).

[38] D. Carlier, J. H. Cheng, R. Berthelot, M. Guignard, M. Yoncheva, R. Stoyanova, B. J. Hwang, and C. Delmas, The P2-$Na_{2/3}Co_{2/3}Mn_{1/3}O_2$ phase: structure, physical properties and electrochemical behavior as positive electrode in sodium battery, Dalton Trans. **40**, 9306–9312 (2011).

[39] R. J. Clément, P. G. Bruce, and C. P. Grey, Review-Manganese-Based P2-Type Transition Metal Oxides as Sodium-Ion Battery Cathode Materials, J. Electrochem. Soc. **162**, A2589–A2604 (2015).

[40] A. Moradabadi and P. Kaghazchi, Mechanism of Li intercalationdeintercalation intofrom the surface of $LiCoO_2$, Phys. Chem. Chem. Phys. **17**, 22917–22922 (2015).

[41] Y. Mo, S. P. Ong, and G. Ceder, Insights into Diffusion Mechanisms in P2 Layered Oxide Materials by First-Principles Calculations, Chem. Mater. **26**, 5208–5214 (2014).

[42] S. Guo, Y. Sun, J. Yi, K. Zhu, P. Liu, Y. Zhu, G.-Z. Zhu, M. Chen, M. Ishida, and H. Zhou, Understanding sodium-ion diffusion in layered P2 and P3 oxides via experiments and first-principles calculations: a bridge between crystal structure and electrochemical performance, NPG Asia Mater. **8**, e266 (2016).

[43] I. Hasa, D. Buchholz, S. Passerini, and J. Hassoun, A Comparative Study of Layered Transition Metal Oxide Cathodes for Application in Sodium-Ion Battery, ACS Appl. Mater. Interfaces **7**, 5206–5212 (2015).

[44] L.-Y. Kuo, A. Moradabadi, H.-F. Huang, B.-J. Hwang, and P. Kaghazchi, Structure and ionic conductivity of the solid electrolyte interphase layer on tin anodes in Na-ion batteries, J. Power Sources **341**, 107–113 (2017).

[45] G. L. W. Hart and R. W. Forcade, Algorithm for generating derivative structures, Phys. Rev. B **77**, 224115 (2008).

[46] A. J. Toumar, S. P. Ong, W. D. Richards, S. Dacek, and G. Ceder, Vacancy Ordering in $O3$-Type Layered Metal Oxide Sodium-Ion Battery Cathodes, Phys. Rev. Applied **4**, 064002 (2015).

[47] Z. Lu, R. A. Donaberger, and J. R. Dahn, Superlattice Ordering of Mn, Ni, and Co in Layered Alkali Transition Metal Oxides with P2, P3, and O3 Structures, Chem. Mater. **12**, 3583–3590 (2000).

[48] A. Jain, S. P. Ong, W. Chen, B. Medasani, X. Qu, M. Kocher, M. Brafman, G. Petretto, G.-M. Rignanese, G. Hautier, D. Gunter, and K. A. Persson, FireWorks: a dynamic workflow system designed for high-throughput applications, Concurrency Computat.: Pract. Exper. **27**, 5037–5059 (2015).

[49] G. Kresse and J. Furthmüller, Efficient iterative schemes for *ab initio* total-energy calculations using a plane-wave basis set, Phys. Rev. B **54**, 11169–11186 (1996).

[50] P. E. Blöchl, Projector augmented-wave method, Phys. Rev. B **50**, 17953–17979 (1994).

[51] J. P. Perdew, K. Burke, and M. Ernzerhof, Generalized gradient approximation made simple, Phys. Rev. Lett. **77**, 3865–3868 (1996).

[52] S. L. Dudarev, G. A. Botton, S. Y. Savrasov, C. J. Humphreys, and A. P. Sutton, Electron-energy-loss spectra and the structural stability of nickel oxide: An LSDA+U study, Phys. Rev. B **57**, 1505–1509 (1998).

[53] L. Wang, T. Maxisch, and G. Ceder, Oxidation energies of transition metal oxides within GGA+U framework, Phys. Rev. B **73**, 195107 (2006).

[54] A. Jain, G. Hautier, S. P. Ong, C. J. Moore, C. C. Fischer, K. A. Persson, and G. Ceder, Formation enthalpies by mixing GGA and GGA+U calculations, Phys. Rev. B **84**, 045115 (2011).

[55] A. Jain, S. P. Ong, G. Hautier, W. Chen, W. D. Richards, S. Dacek, S. Cholia, D. Gunter, D. Skinner, G. Ceder, and K. A. Persson, Commentary: The Materials Project: A materials genome approach to accelerating materials innovation, APL Mater. **1**, 011002 (2013).

[56] J. Su, Y. Pei, Z. Yang, and X. Wang, First-principles investigation on the structural, electronic properties and diffusion barriers of MgAl doped $NaCoO_2$ as the cathode material of rechargeable sodium batteries, RSC Adv. **5**, 27229–27234 (2015).

[57] S. P. Ong, L. Wang, B. Kang, and G. Ceder, Li-Fe-P-O_2 Phase Diagram from First Principles Calculations, Chem. Mater. **20**, 1798–1807 (2008).

[58] M. K. Aydinol, A. F. Kohan, G. Ceder, K. Cho, and J. Joannopoulos, *Ab initio* study of lithium intercalation in metal oxides and metal dichalcogenides, Phys. Rev. B **56**, 1354–1365 (1997).

[59] S. Nos, A unified formulation of the constant temperature molecular dynamics methods, J. Chem. Phys. **81**, 511–519 (1984).

[60] W. G. Hoover, Canonical dynamics: Equilibrium phase-space distributions, Phys. Rev. A **31**, 1695–1697 (1985).

[61] G. Henkelman, B. P. Uberuaga, and H. Jnsson, A climbing image nudged elastic band method for finding saddle points and minimum energy paths, J. Chem. Phys. **113**, 9901–9904 (2000).

[62] G. Henkelman and H. Jnsson, Improved tangent estimate in the nudged elastic band method for finding minimum energy paths and saddle points, J. Chem. Phys. **113**, 9978 (2000).

[63] S. P. Ong, W. D. Richards, A. Jain, G. Hautier, M. Kocher, S. Cholia, D. Gunter, V. L. Chevrier, K. A. Persson, and G. Ceder, Python materials genomics (pymatgen): A robust, open-source python library for materials analysis, Computational Materials Science **68**, 314 – 319 (2013).

[64] H. W. Zandbergen, M. Foo, Q. Xu, V. Kumar, and R. J. Cava, Sodium ion ordering in Na_xCoO_2: Electron diffraction study, Phys. Rev. B **70**, 024101 (2004).

[65] F. Zhou, M. Cococcioni, C. A. Marianetti, D. Morgan, and G. Ceder, First-principles prediction of redox potentials in transition-metal compounds with LDA+U, Phys. Rev. B **70**, 235121 (2004).

[66] X. Li, X. Ma, D. Su, L. Liu, R. Chisnell, S. P. Ong, H. Chen, A. Toumar, J.-C. Idrobo, Y. Lei, J. Bai, F. Wang, J. W. Lynn, Y. S. Lee, and G. Ceder, Direct visualization of the Jahn-Teller effect coupled to Na ordering in $Na_{5/8}MnO_2$, Nat. Mater. **13**, 586–92 (2014).

[67] C. Ouyang, S. Shi, and M. Lei, Jahn-Teller distortion and electronic structure of $LiMn_2O_4$, J. Alloys Compd. **474**, 370 – 374 (2009).

[68] X. Ma, H. Chen, and G. Ceder, Electrochemical Properties of Monoclinic $NaMnO_2$, J. Electrochem. Soc. **158**, A1307–A1312 (2011).

[69] A. Mendiboure, C. Delmas, and P. Hagenmuller, Electrochemical intercalation and deintercalation of Na_xMnO_2 bronzes, J. Solid State Chem. **57**, 323 – 331 (1985).

[70] J. Sanchez, F. Ducastelle, and D. Gratias, Generalized cluster description of multicomponent systems, Phys. A **128**, 334 – 350 (1984).

[71] A. Van der Ven and G. Ceder, Lithium Diffusion in Layered Li_xCoO_2, Electrochem. Solid-State Lett. **3**, 301–304 (2000).

[72] M. F. Sykes and J. W. Essam, Exact Critical Percolation Probabilities for Site and Bond Problems in Two Dimensions, J. Math. Phys. **5**, 1117–1127 (1964).

[73] S. Doubaji, M. Valvo, I. Saadoune, M. Dahbi, and K. Edström, Synthesis and characterization of a new layered cathode material for sodium ion batteries, J. Power Sources **266**, 275–281 (2014).

[74] D. Yuan, W. He, F. Pei, F. Wu, Y. Wu, J. Qian, Y. Cao, X. Ai, and H. Yang, Synthesis and electrochemical behaviors of layered $Na_{0.67}[Mn_{0.65}Co_{0.2}Ni_{0.15}]O_2$ microflakes as a stable cathode material for sodium-ion batteries, J. Mater. Chem. A **1**, 3895–3899 (2013).

[75] D. Buchholz, L. G. Chagas, M. Winter, and S. Passerini, P2-type layered $Na_{0.45}Ni_{0.22}Co_{0.11}Mn_{0.66}O_2$ as intercalation host material for lithium and sodium batteries, Electrochim. Acta **110**, 208–213 (2013).

[76] J. Yoshida, E. Guerin, M. Arnault, C. Constantin, B. Mortemard de Boisse, D. Carlier, M. Guignard, and C. Delmas, New P2-$Na_{0.70}Mn_{0.60}Ni_{0.30}Co_{0.10}O_2$ Layered Oxide as Electrode Material for Na-Ion Batteries, J. Electrochem. Soc. **161**, A1987–A1991 (2014).

[77] H. Wang, B. Yang, X.-Z. Liao, J. Xu, D. Yang, Y.-S. He, and Z.-F. Ma, Electrochemical properties of P2-$Na_{2/3}[Ni_{1/3}Mn_{2/3}]O_2$ cathode material for sodium ion batteries when cycled in different voltage ranges, Electrochim. Acta **113**, 200–204 (2013).

[78] T. Shibata, Y. Fukuzumi, W. Kobayashi, and Y. Moritomo, Fast discharge process of layered cobalt oxides due to high Na^+ diffusion, Sci. Rep. **5**, 9006 (2015).

[79] K. Kang, Y. S. Meng, J. Bréger, C. P. Grey, and G. Ceder, Electrodes with High Power and High Capacity for Rechargeable Lithium Batteries, Science **311**, 977–980 (2006).

[80] A. Van der Ven, G. Ceder, M. Asta, and P. D. Tepesch, First-principles theory of ionic diffusion with nondilute carriers, Phys. Rev. B **64**, 184307 (2001).

[81] See Supplemental Material at [url] for the effect of Co-Mn framework on Na ordering. Na migration energy barrier calculation; stable Na orderings of Na_xMnO_2 predicted using the PBE and PBE+U functionals. PBE 0K stability diagrams of $Na_xCo_{2/3}Mn_{1/3}O_2$ and $Na_xCo_{1/3}Mn_{2/3}O_2$. PBE and PBE+U 0K stability diagrams of Na_xMnO_2. PBE and PBE+U voltage profiles of Na_xMnO_2. Convergence of Na site occupancies and average Na site occupancy fractions of P2 $Na_xCo_{1-y}Mn_yO_2$ during AIMD simulations. Na migration barriers calculated using $Na_xCo_{2/3}Mn_{1/3}O_2$.

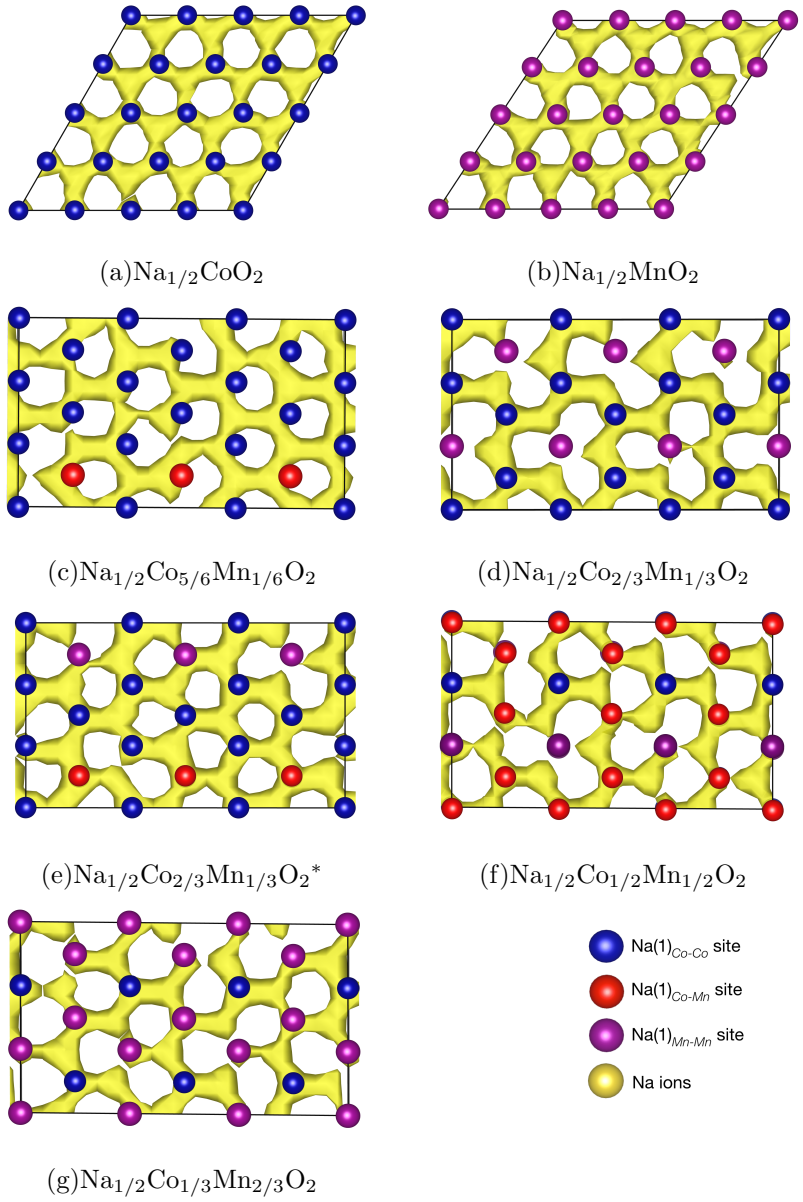

FIG. 5: Isosurfaces of Na ion (yellow) probability density distribution P at $P = P_{max}/12$ for P2 $Na_{1/2}Co_{1-y}Mn_yO_2$ at 1000 K, top view from AB plane. Metallic blue dots indicate the positions of $Na(1)_{Co-Co}$ sites and red dots represent the positions of $Na(1)_{Co-Mn}$ sites. Magenta circles correspond to $Na(1)_{Mn-Mn}$ sites' positions. All simulations were carried out using ground-state Co-Mn frameworks of P2 $Na_{1/2}Co_{1-y}Mn_yO_2$ except $Na_{1/2}Co_{2/3}Mn_{1/3}O_2{}^*$ in Figure 5(e). $Na_{1/2}Co_{2/3}Mn_{1/3}O_2{}^*$ framework in Figure 5(e) was randomized such that it contains all three types of Na(1) site. This framework is different from the ground state Co-Mn framework of $Na_{1/2}Co_{2/3}Mn_{1/3}O_2$ as shown in Figure S6(a).

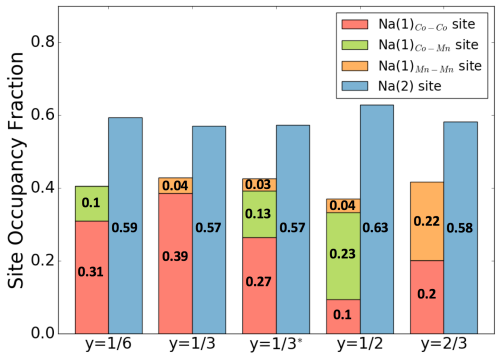

FIG. 6: (color online) Average Na site occupancy fractions (SOFs) in P2 $Na_{1/2}Co_{1-y}Mn_yO_2$ from AIMD simulations at 1000K. The average SOFs are estimated from 25 ps AIMD simulation results. All AIMD simulations were carried out using ground-state Co-Mn frameworks of P2 $Na_{1/2}Co_{1-y}Mn_yO_2$ except $y = 1/3^*$, in which the Co-Mn ordering was randomized such that it contains all four types of Na sites.

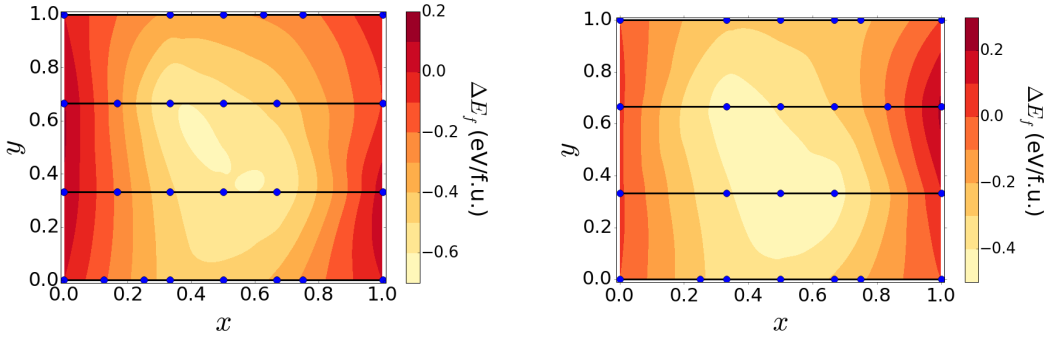

(a)PBE (b)PBE+U

FIG. 7: (color online) P2 $Na_xCo_{1-y}Mn_yO_2$ 0K stability diagrams calculated using (a) PBE and (b) PBE+U. Stable orderings are indicated by blue circles. Background color indicates the formation energy per formula unit with respect to the fully sodiated and fully desodiated structures. See text for details.

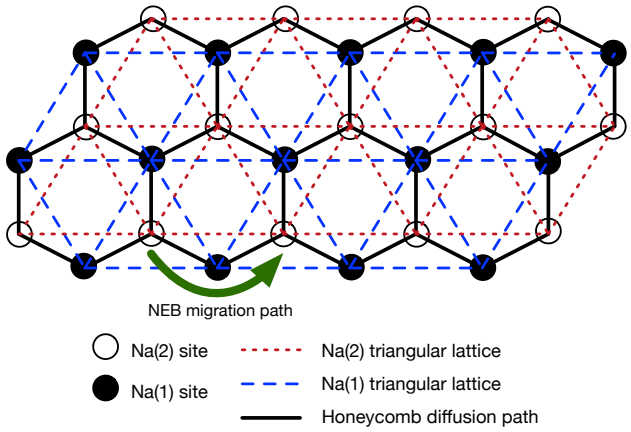

FIG. 8: Schematic view of 2D Na diffusion pathways (top view on AB plane) consisted of triangular lattices. Black dots are Na(1) sites. White circles represent Na(2) sites. Solid black lines highlight the two-dimensional honeycomb-like diffusion pathways. Red dash lines show triangular lattices formed by Na(2) sites. Blue dash lines show triangular lattices consisted of Na(1) sites. Green arrows represent the Na migration pathway between two nearest neighbor Na(2) sites via Na(1) site from CI-NEB calculations.